CHAPTER 3

IXORA COCCINEA EXTRACT: NATURAL CORROSION INHIBITOR FOR MILD STEEL IN ACID MEDIA

This chapter delineates the corrosion inhibition power of an eco-friendly green inhibitor *Ixora coccinea* extract (ICE), for mild steel in 1 M HCl and 0.5 M H_2SO_4 using various corrosion monitoring techniques. The major chemical constituent of *Ixora coccinea* leaves ixorene[144] (Fig. 3.1), subjected to theoretical calculations to evaluate the corrosion inhibition ability of the leaf extract in more detail.

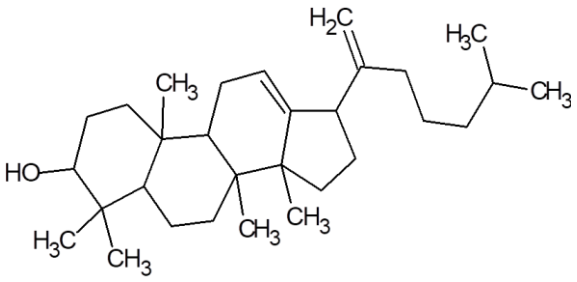

Fig. 3.1: Structure of ixorene

Ixora coccinea

Results and Discussion

Phytochemical screening of ICE

Standard identification tests were conducted to realize the phytochemicals present in ICE, and the results are given in Table 3.1.

FTIR spectroscopy

To identify the functional groups existing in ICE, FTIR spectroscopy of dried powdered *Ixora coccinea* leaves has been examined, shown in Fig. 3.2. A broad band observed at 3438 cm^{-1} indicates O-H stretching vibration. Two strong peaks at 2928 cm^{-1} and 2850 cm^{-1} are pointed alkyl C-H stretching bonds. The peaks at 1628 cm^{-1} and 1384 cm^{-1} represent aliphatic and aromatic C=C stretching bonds, respectively. The other significant peaks indicate the presence of minor components present in ICE.

Table 3.1 Phytochemical screening of ICE

Sl. No.	Compounds	Tests	Results
1	Alkaloids	Mayer's reagent	++
2	Steroids	Salkowaski's test	++
3	Phenolic compounds	Potassium ferrocyanide test	++
4	Flavanoids	Sodium hydroxide test	++
5	Saponins	Froth test	++
6	Tannins	Lead acetate test	––
7	Cardiac glycosides	Conc. sulphuric acid test	++
8	Coumarin	Alcoholic NaOH test	++
9	Quinones	Conc. sulphuric acid test	++

++ (present), – – (Absent)

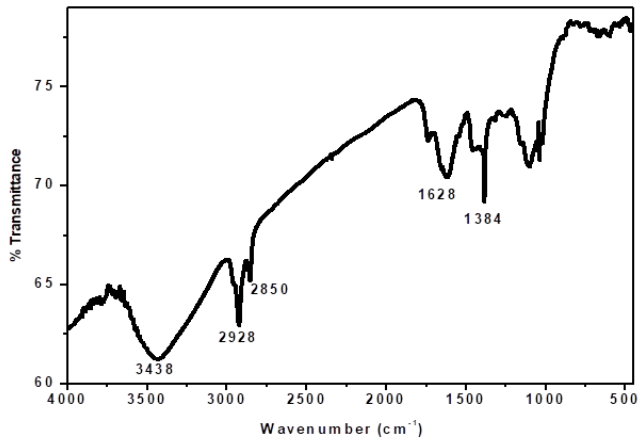

Fig. 3.2: FTIR spectrum of ICE

Weight loss measurements

❖ ***Effect of concentration***

The weight loss measurements of mild steel in 1 M HCl and 0.5 M H_2SO_4 solutions at room temperature with and without various concentrations (1-5 v/v %) of ICE for 24 hrs are recorded in Table 3.2. It is evident from the data that as the concentration of inhibitor is increased, the percentage inhibition efficiency also increases in both the acidic media. The results show that ICE is an efficient inhibitor in 1 M HCl, attaining maximum inhibition efficiency at 5% as 89.38%. This is because the

number of adsorbed organic molecules of inhibitor ICE on mild steel is more in HCl than H_2SO_4 medium.

Table 3.2: Weight loss measurements of mild steel with and without ICE in 1 M HCl and 0.5 M H_2SO_4 at room temperature for 24 hrs

Conc. (v/v %)	Corrosion rate (mm/yr)		Inhibition efficiency (η%)	
	1 M HCl	0.5 M H_2SO_4	1 M HCl	0.5 M H_2SO_4
Blank	3.95	35.57	-	-
1	0.60	12.23	84.77	65.61
2	0.56	11.52	85.75	67.58
3	0.52	9.05	86.73	74.53
4	0.47	8.77	87.98	75.32
5	0.41	7.83	89.38	77.96

❖ ***Effect of temperature***

Effect of temperature on the stability of the adsorption film formed by ICE on mild steel surface was explained by weight loss measurements in 1 M HCl and 0.5 M H_2SO_4 at elevated temperatures for 24 hrs. Inhibition efficacy was calculated and given in Table 3.3 and is graphically depicted in Fig. 3.3. Inhibition efficiency obtained for the highest concentration (5 v/v%) is 89.38 % in 1 M HCl. But when the temperature increases by 10 K, the efficiency lowered to 88.93 % and then went to 66.03 % for a further rise of 10 K, finally reaches 51.14% at the highest temperature (333 K). Similarly, in the case of 0.5 M H_2SO_4, the rate of corrosion enhances at elevated temperatures for the same concentration. This may be attributed to the instability of adsorbed film at higher temperatures. Higher temperature may cause desorption on the metal surface[58]. This indicates ICE molecules adsorb on the mild steel surface mainly by physisorption. So, temperature influences the action of inhibitor on the metal surface and thereby corrosion control.

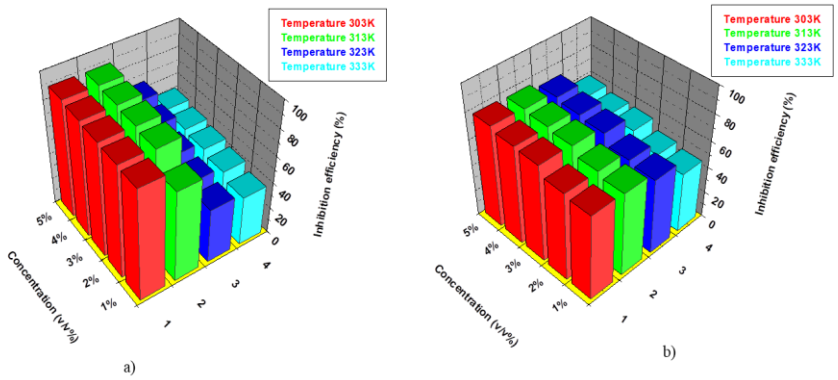

Fig. 3.3: Variation in inhibition efficiency of ICE in a) 1 M HCl b) 0.5 M H_2SO_4 at elevated temperatures

Table 3.3: Corrosion rate (υ) and inhibition efficiency (η%) of ICE in 1 M HCl and 0.5 M H_2SO_4 at different temperatures for 24 hrs

Medium	Conc. (v/v%)	υ (303 K)	η% (303 K)	υ (313 K)	η% (313 K)	υ (323 K)	η% (323 K)	υ (333K)	η% (333 K)
1 M HCl	Blank	3.95	-	13.11		22.05	-	31.77	-
	1	0.60	84.77	4.04	69.18	12.82	41.85	19.89	37.39
	2	0.56	85.75	2.06	84.28	11.68	47.02	18.19	42.74
	3	0.52	86.73	1.80	86.27	10.50	52.38	17.09	46.20
	4	0.47	87.98	1.59	87.87	8.62	60.90	16.43	48.28
	5	0.41	89.38	1.45	88.93	7.49	66.03	15.52	51.14
0.5 M H_2SO_4	Blank	35.57	-	58.27	-	86.25	-	106.2	-
	1	12.23	65.61	20.70	64.47	36.39	57.80	57.35	46.02
	2	11.52	67.58	19.05	67.30	34.44	60.06	54.47	48.73
	3	9.05	74.53	15.50	73.39	27.90	67.65	47.09	55.68
	4	8.77	75.32	14.49	75.13	25.99	69.86	45.99	56.71
	5	7.83	77.96	13.51	76.81	23.97	72.20	42.98	59.55

Using Arrhenius equation (41), plots of log K vs 1/T for metal corrosion in the presence and absence of ICE in acid media were obtained and are shown in Fig. 3.4 a) and Fig. 3.5 a). Activation energy of corrosion in acid media was calculated from the slopes of the plots. From transition state theory, thermodynamic parameters such as enthalpy of activation (ΔH^*) and entropy of activation (ΔS^*) were equated as in the equation (42). Fig. 3.4 b) and Fig. 3.5 b) show Arrhenius plots of log K/T vs 1/T. ΔH^* and ΔS^* values were derived from these plots and are given in Table 3.4 along with activation energy (E_a) and Arrhenius factor (A).

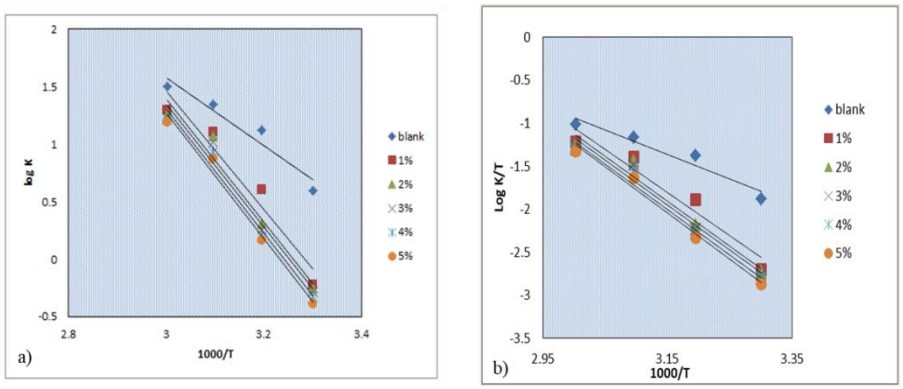

Fig. 3.4: Arrhenius plots of a) log K vs 1000/T b) log K/T vs 1000/T in the presence and absence of ICE in 1 M HCl

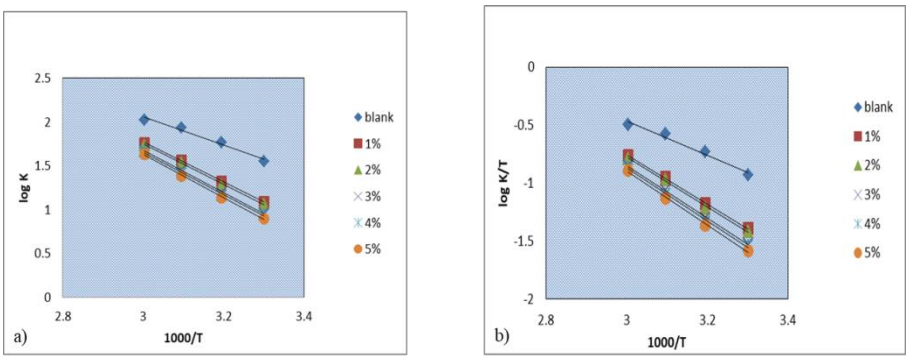

Fig. 3.5: Arrhenius plots of a) log K vs 1000/T b) log K/T vs 1000/T in the presence and absence of ICE in 0.5 M H_2SO_4

It exhibited that as the concentration of ICE increases, the activation energy of corrosion also enhances in both acids. This can be ascribed to the growing energy barrier with the increase in ICE concentration. It was evident that an activated complex compound was formed by the interaction of the inhibitor with mild steel. Positive enthalpy values were indicated that the corrosion process was endothermic. The values of ΔS* were also found to be raised as ICE concentration increases. Entropy of activation for corrosion was observed to be negative for blank solution mentioned that a decrease in randomness for the activated complex, compared to the reactants[145]. In the presence of ICE, the disorderliness of the activated complex getting increased, and ΔS* values became positive in the HCl medium. In the case of 0.5 M H_2SO_4, ΔS* values became less negative with increased ICE concentration.

Table 3.4: Thermodynamic parameters of mild steel corrosion with and without ICE in 1 M HCl and 0.5 M H_2SO_4

Medium	Conc. (v/v%)	E_a (kJ mol^{-1})	A	ΔH^* (kJ mol^{-1})	ΔS^* (J $mol^{-1}K^{-1}$)
1 M HCl	Blank	57.25	$3.58X10^{10}$	54.60	-44.77
	1	98.52	$7.94X10^{16}$	95.90	76.73
	2	102.55	$2.89X10^{17}$	99.90	87.47
	3	103.03	$3.16X10^{17}$	100.0	88.20
	4	103.87	$3.87X10^{17}$	101.0	89.88
	5	105.45	$6.32X10^{17}$	103.0	93.88
0.5 M H_2SO_4	Blank	30.96	8167704	28.30	-114.51
	1	43.64	$4.04X10^{8}$	41.00	-82.05
	2	44.06	$4.47X10^{8}$	41.40	-81.22
	3	46.42	$8.92X10^{8}$	43.80	-75.48
	4	46.54	$8.91X10^{8}$	43.90	-75.49
	5	47.62	$1.23X10^{9}$	45.00	-72.80

Adsorption isotherms

Mechanism of corrosion inhibition between inhibitor molecules and mild steel metal was illustrated using adsorption isotherms. Several adsorption isotherms like Langmuir, El-Awady, Frumkin, Temkin, Freundlich, and Flory-Huggins were considered for the study. The best suitable isotherm was detected using the value of the correlation coefficient (R^2).

From the values of R^2 in Fig. 3.6, it can be seen that Langmuir adsorption isotherm is the best suitable one for the adsorption of ICE on mild steel. The ΔG^0_{ads} calculated for ICE is -32.88 and -29.58 kJ/mol in 1 M HCl and 0.5 M H_2SO_4, respectively, showing that an electrostatic and chemical interaction exists between the inhibitor and the charged metal surface. ICE is composed of various organic compounds. The significant component of *Ixora coccinea* leaves is ixorene. Adsorption of all the ICE components on the mild steel surface may be attributed to the inhibitive action of the extract. Fig. 3.7 represents the predominant interaction of the significant component ixorene with the mild steel surface. By transferring electrons from the oxygen atom

present in -OH group and the interaction through the double bonds, ixorene molecules can be adsorbed onto the mild steel surface.

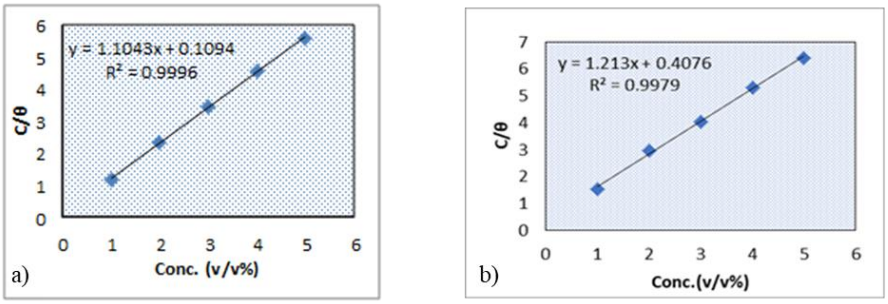

Fig. 3.6: Langmuir adsorption isotherm of ICE on mild steel in a) 1 M HCl b) 0.5 M H_2SO_4 at room temperature

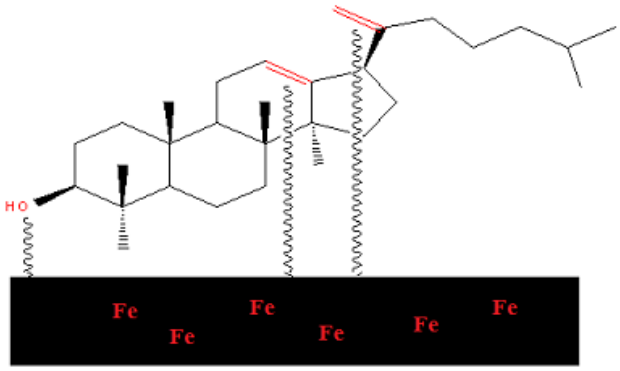

Fig. 3.7: Interaction diagram between ixorene and mild steel surface in acid media

UV-Visible spectroscopy

Metal-inhibitor interaction can be further established by studying UV-Visible spectroscopy. UV-Visible spectra were plotted for a) 5 ppm ICE, b) 5 ppm metal salt solution and c) equal proportions of the metal salt and ICE (Fig. 3.8). The UV spectrum of ICE exhibits a maximum absorbance of 2.045 at 666 nm. There is a sharp decrease in the intensity of ICE after binding with all the metal salts under study. In the case of $CoCl_2$, the maximum absorbance of 0.874 at 666 nm shows 57% decrease in the intensity after binding. In the case of chromium (III) acetate, the maximum absorbance of 1.208 at 666 nm exhibits 40% decrease in the intensity after binding. NaCl and Mn(II) acetate show almost the same reduction in intensity (51%) at 666 nm. Zn(II) acetate and Fe(III) chloride exhibit 1.053 and 1.018 at 666 nm, respectively indicates 50% decrease in

intensity. A significant reduction in intensity (58%) was observed in Cu(II) acetate as a maximum absorbance of 0.857 at 666 nm. This quenching may account for the strong affinity of ICE towards metal salts[146]. Thus, UV-Visible spectral studies prove the metal binding ability of ICE molecules.

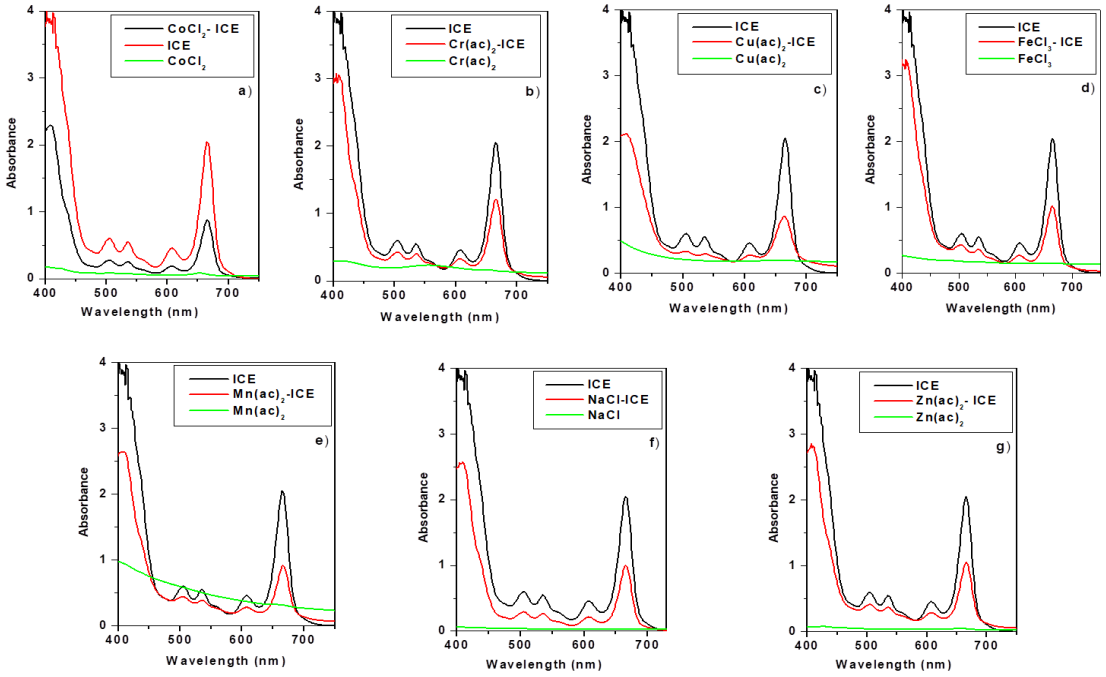

Fig. 3.8: UV spectra of a) ICE, $CoCl_2$ and ICE.$CoCl_2$ b) ICE, $Cr(ac)_2$ and ICE.$Cr(ac)_2$ c) ICE, $Cu(ac)_2$ and ICE.$Cu(ac)_2$ d) ICE, $FeCl_3$ and ICE.$FeCl_3$ e) ICE, $Mn(ac)_2$ and ICE.$Mn(ac)_2$ f) ICE, NaCl and ICE.NaCl g) ICE, $Zn(ac)_2$ and ICE.$Zn(ac)_2$

Electrochemical impedance spectroscopy

The equivalent circuit employed in this study is Randle's circuit (Fig. 1.8). It includes solution resistance R_s, charge transfer resistance R_{ct} and double layer capacitance C_{dl}. The deformities on the metal surface cause deviations from the ideal dielectric property of the metal. So, a constant phase element (Z) is preferred to C_{dl}[147].

$$Z = Q^{-1}(j\omega)^{-n} \qquad (51)$$

where Q is the measure of constant phase element, n is the power of the magnitude of constant phase element, ω is the angular frequency, and j is the imaginary unit. Based on the values of n, Z may be a resistance value.

Nyquist and Bode plots of mild steel without and with the inhibitor ICE using various concentrations (1-5 v/v %) in 1 M HCl and 0.5 M H_2SO_4 at room temperature are shown in Fig. 3.9 & Fig. 3.10. In Nyquist plots, it was seen that the low-frequency region is plotted to a straight line, and the high-frequency region is plotted to a semi-circle. The slight fall in the semi-circular plot may be ascribed to the heterogeneous and roughness of the mild steel. The straight-line portion represented the diffusion from the solution[148]. As the concentration of ICE is raised, the size of the loop also increases. This can be ascribed to the increase in the impedance of inhibited mild steel. The efficiency also increases in the process.

Table 3.5: Impedance parameters of mild steel in 1 M HCl and 0.5 M H_2SO_4 with and without ICE

Conc. (v/v%)	1 M HCl			0.5 M H_2SO_4		
	R_{ct} (Ωcm^2)	C_{dl} (μFcm^{-2})	η_{EIS}%	R_{ct} (Ωcm^2)	C_{dl} (μFcm^{-2})	η_{EIS}%
Blank	15.7	78.8	-	18.1	47.4	-
1	69.7	57.4	77.47	20.3	50.5	10.83
2	73.9	49.6	78.74	37.4	39.0	51.56
3	86.4	49.7	81.82	44.1	36.9	58.93
4	150	48.5	89.53	85.5	28.3	78.83
5	186	43.6	91.55	187	3.43	90.33

Impedance data obtained from the above equivalent circuit for both media are given in Table 3.5. On analyzing the data in Table 3.5, it has been noted that R_{ct} values were increased on the addition of ICE. It may be due to the increase in the rate of adsorption of ICE on the metal surface. As the concentration of inhibitor increases, double-layer capacitance (C_{dl}) decreases, which indicates that the thickness of the electrical double layer increases with respect to the concentration. This is due to the adsorption of inhibitor molecules on the mild steel surface[149]. The maximum inhibition

efficiency of 91.55% was seen at 5% concentration of ICE in 1 M HCl and 90.33% in 0.5 M H_2SO_4 at the same ICE concentration. From the impedance parameters, it was clear that ICE acted as a suitable corrosion inhibitor in both acid media. This result was matched with weight loss measurements.

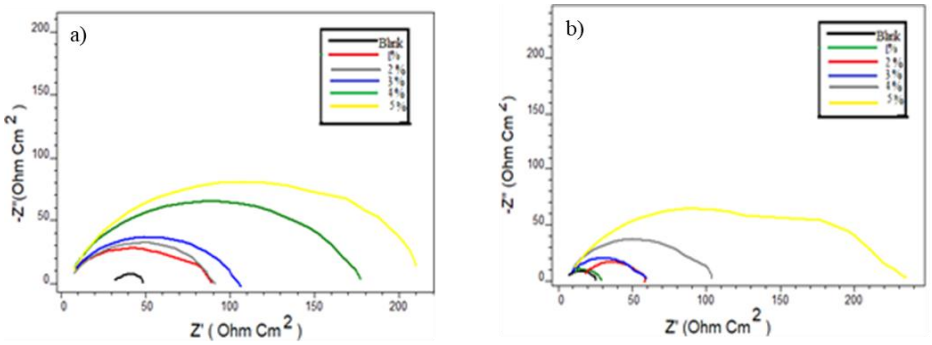

Fig. 3.9: Nyquist plots of mild steel with and without ICE in a) 1 M HCl and b) 0.5 M H_2SO_4

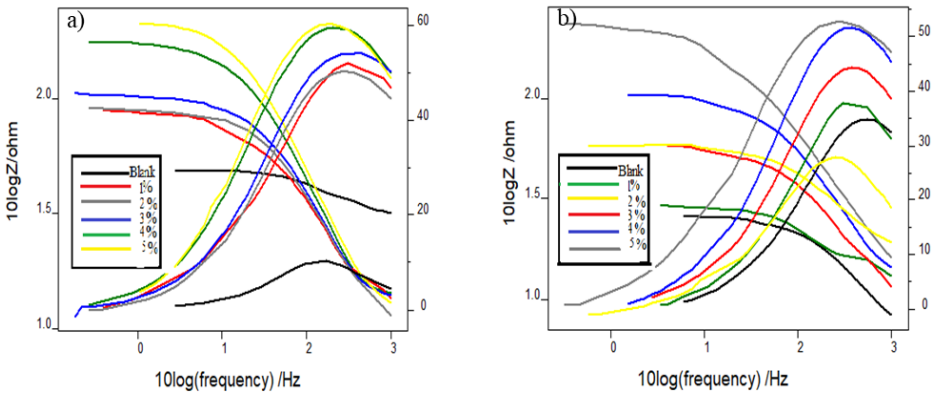

Fig. 3.10: Bode plots of mild steel with and without ICE in a) 1 M HCl and b) 0.5 M H_2SO_4

Potentiodynamic polarization studies

The potentiodynamic polarization data of mild steel in 1 M HCl and 0.5 M H_2SO_4 with and without ICE are given in Table 3.6, and corresponding Tafel plots are depicted in Fig. 3.11. Linear polarization curves are pictured in Fig. 3.12.

The potentiodynamic polarization data revealed that the greater the ICE concentration, the smaller is the corrosion current density (i_{corr}). The inhibition efficiency was also seen to increase. The inhibition efficiency of ICE for mild steel reached an upper limit of 93.67% in 1 M HCl solution and 87.02% in 0.5 M H_2SO_4 solution at higher

concentrations. From the slopes of Tafel plots, it is seen that both cathodic and anodic curves were influenced by the addition of various concentrations of ICE, which shows the mixed type inhibition character of ICE in both acids[150]. Linear polarization data were also reinforced with Tafel data.

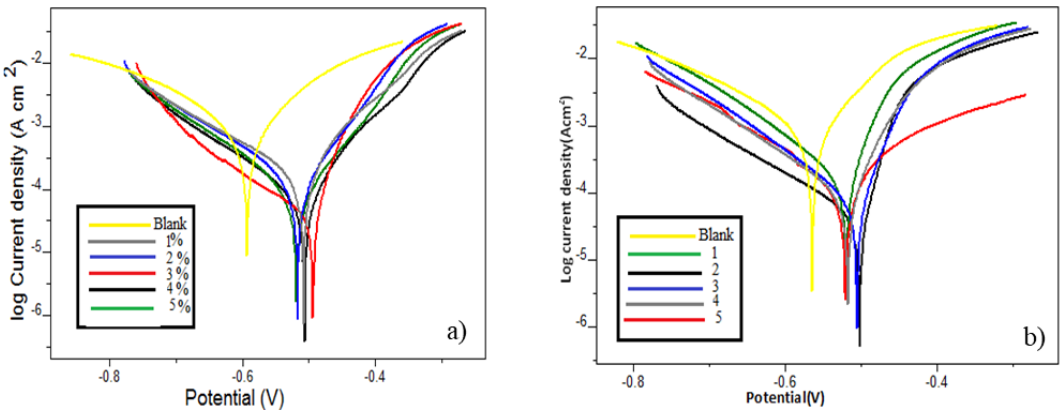

Fig. 3.11: a) Tafel plots of mild steel with and without ICE in a) 1 M HCl and b) 0.5 M H_2SO_4

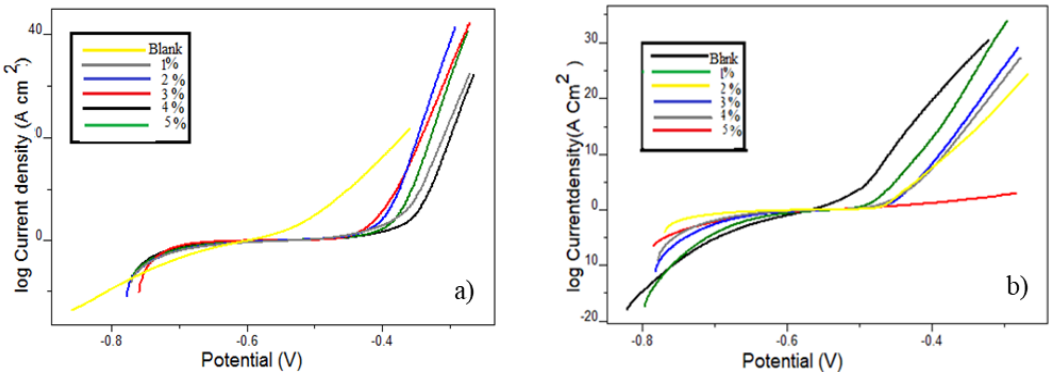

Fig. 3.12: Linear polarization plots of mild steel with and without ICE in a) 1 M HCl and b) 0.5 M H_2SO_4

Moreover, E_{corr} values of inhibited solution didn't vary noticeably (>85) regarding the blank solution. This trend was also assisted the mixed type inhibition character of ICE in acid media.

Electrochemical noise measurements

Fig. 3.13 represents the current noise for mild steel with and without various ICE concentrations (1, 3, 5 v/v %) in 1 M HCl and 0.5 M H_2SO_4. For inhibitor molecules, current and potential noise is lower than the uninhibited system. It was seen that

protecting power of ICE is increased as its concentration increases. Higher magnitude of potential noise signal of uninhibited acid media indicates appreciable localized metallic corrosion on the metal surface[151].

Table 3.6: Potentiodynamic polarization parameters of mild steel in 1 M HCl and 0.5 M H_2SO_4 with and without ICE

Medium	Conc. (v/v%)	Tafel data					Polarization data	
		E_{corr} (mV)	i_{corr} ($\mu A/cm^2$)	b_a (mV/dec)	$-b_c$ (mV/dec)	$\%\eta_{pol}$	R_p (ohm)	$\%\eta_{Rp}$
1 M HCl	Blank	-597.9	1240	166	221	-	33.14	
	1	-522.8	193.6	106	170	84.41	146.3	77.34
	2	-504.8	122.3	69	158	90.11	170.4	80.55
	3	-571.6	107.9	100	130	91.29	228.1	85.47
	4	-515.0	87.22	93	149	92.96	260.6	87.28
	5	-500.7	78.50	69	146	93.67	284.4	88.34
0.5 M H_2SO_4	Blank	-602.2	1616	184	193	-	25.3	
	1	-601.8	811.6	170	136	49.77	40.46	37.46
	2	-649.6	415.5	199	156	74.28	79.39	68.13
	3	-588.9	368.4	142	128	77.20	91.42	72.32
	4	-587.4	306.9	138	137	81.00	97.12	73.94
	5	-555.7	209.6	221	142	87.02	179.3	85.88

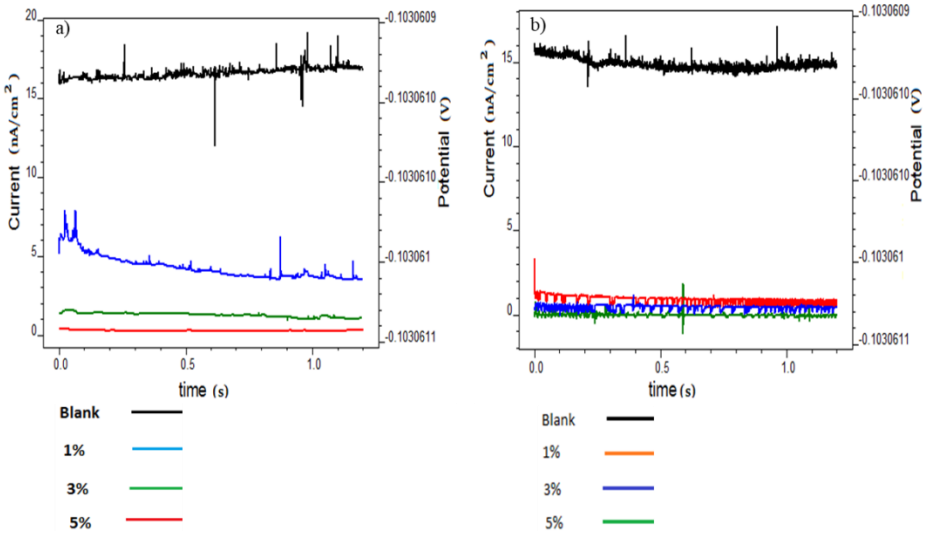

Fig. 3.13: Current noise plots of mild steel with and without ICE in a) 1 M HCl b) 0.5 M H_2SO_4

Power spectral density (PSD) was furnished by the frequency domain analysis of noise parameters. PSD plots in Fig. 3.14 revealed that the magnitude of the signals is higher for blank metal than metals with various concentrations of ICE (1, 3, 5 v/v %) in 1 M HCl and 0.5 M H_2SO_4. This indicated a considerable amount of localized corrosion on

the mild steel surface in the absence of ICE. As the concentration of ICE become greater, the magnitude of the noise signal decreases, showing its anti-corrosion property against mild steel in both acid solutions.

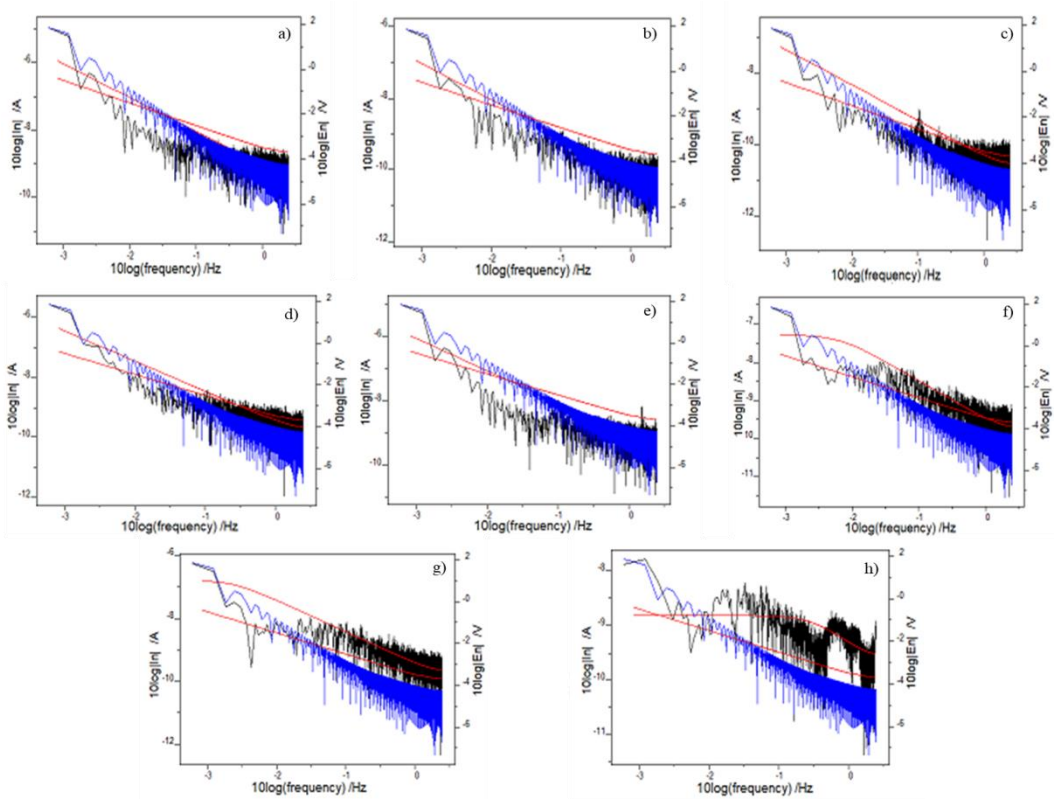

Fig. 3.14: Power spectral density plots of mild steel in 1 M HCl a) without ICE b) 1% ICE c) 3% ICE d) 5% ICE; Power spectral density plots of mild steel in 0.5 M H_2SO_4 e) without ICE f) 1% ICE g) 3% ICE h) 5% ICE

The extent of pitting corrosion can be understood by the pitting index value. Fig. 3.15 depicts pitting index curves for mild steel corrosion in 1 M HCl and 0.5 M H_2SO_4 in the presence and absence of various concentrations of ICE. Pitting index value of the mild steel in the blank solution of HCl was found to be minor, whereas its value was increased by adding 1, 3 and 5 v/v% ICE concentration and attained a higher value at the highest concentration under study. Similarly, in the blank experiment using 0.5 M H_2SO_4 solution, the pitting index value was lower and increased with various ICE concentrations. The high value of the pitting index indicated the strong resistance power of ICE molecules against pitting corrosion of mild steel in 1 M HCl and 0.5 M H_2SO_4[152].

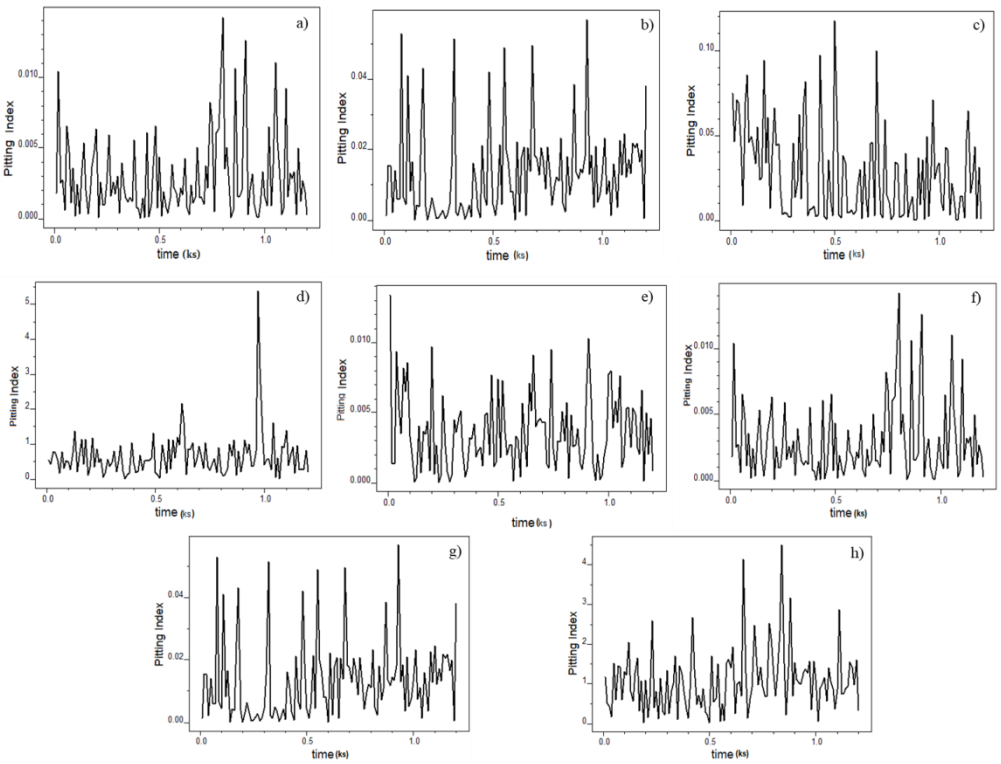

Fig. 3.15: Pitting index curves of mild steel in 1 M HCl a) without ICE b) 1% ICE c) 3% ICE d) 5% ICE; Pitting index curves of mild steel in 0.5 M H_2SO_4 e) without ICE f) 1% ICE g) 3% ICE h) 5% ICE

Scanning electron microscopy

To strengthen the understanding of the mechanism of ICE on the surface of mild steel, morphological studies were performed by taking the SEM images of metal coupons[153]. Fig. 3.16 a) shows the SEM picture of smoothening mild steel metal. Fig. 3.16 b, c, d, e shows the surface of mild steel metal after immersion in 1 M HCl and 0.5 M H_2SO_4, respectively, without and with ICE. The SEM images clearly exhibited that the surface is severely damaged in the absence of the inhibitor ICE. It could be seen that the surface corrosion is getting reduced in HCl solution with ICE and the surface is more smooth and perfect in it than H_2SO_4 solution. So it can be confirmed that ICE acts as an excellent green corrosion inhibitor in acidic media.

Quantum mechanical calculations

Quantum mechanical parameters like E_{HOMO}, E_{LUMO}, ΔE, Ionisation energy (I), Electron affinity (A), Chemical potential (μ), electronegativity (χ), hardness (η) and the

number of transferred electrons (ΔN) of ixorene are tabulated in Table 3.7. The HOMO and LUMO pictures of ixorene are depicted in Fig. 3.17. The ΔE value was found to be low for ixorene, which indicated that ICE has remarkable inhibition efficiency. The low ΔE value 4.884 eV of ixorene can be attributed to the low energy requirement for transferring electrons from HOMO of ixorene to the vacant orbitals of Fe. The high E_{HOMO} value (3.347) and low E_{LUMO} value (1.537) of ixorene were facilitated the strong interaction of inhibitor molecules on the mild steel surface[154]. The number of electrons transferred (ΔN) from inhibitor to metal can be calculated using equation (49) by assuming that chemical hardness and electronegativity of Fe metal is zero and 7 eV, respectively. The ΔN value of ixorene calculated as 1.2479 pointed out the interaction between donor-acceptor molecules. This, in turn, proved agreement between quantum mechanical calculations and experimental results.

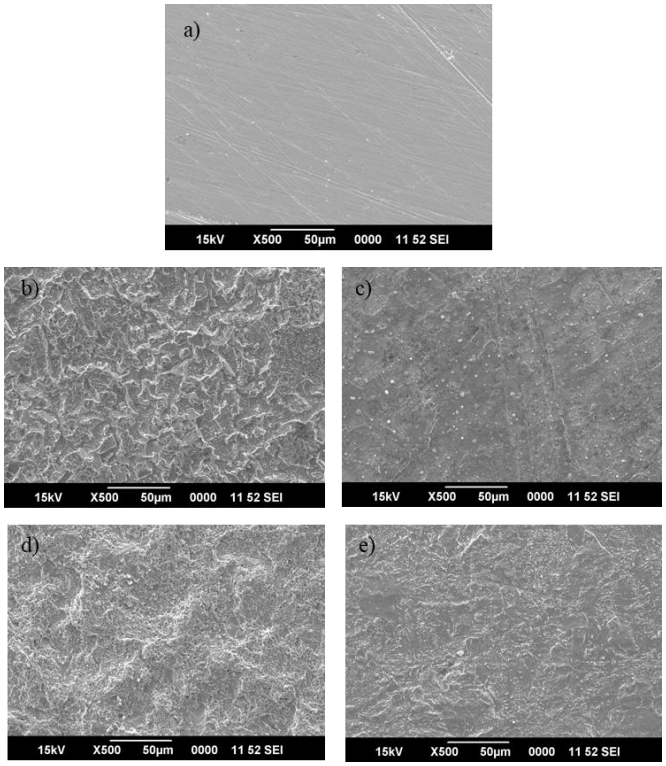

Fig. 3.16: SEM images of the surface of mild steel a) bare b) in 1 M HCl c) in 1 M HCl with ICE d) in 0.5 M H_2SO_4 e) in 0.5 M H_2SO_4 with ICE

Table 3.7: Quantum mechanical parameters (in eV) of ixorene

E_{HOMO}	E_{LUMO}	ΔE	I	A	μ	χ	η	ΔN
-3.347	1.537	4.884	3.347	-1.537	-0.905	0.905	2.442	1.2479

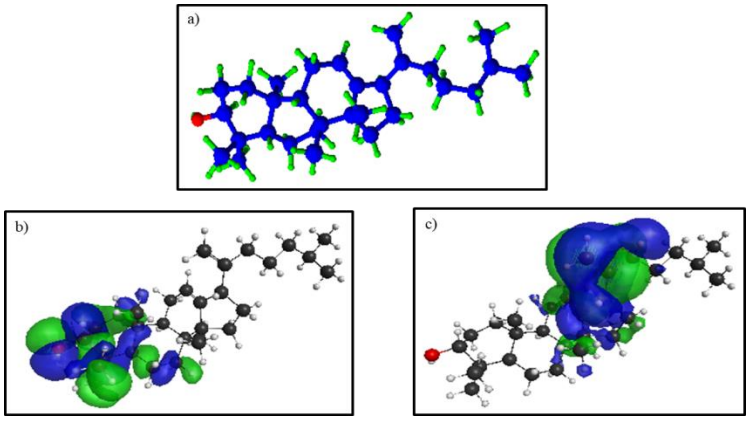

Fig. 3.17: a) Optimized geometry, b) HOMO and c) LUMO of ixorene

Statistical analysis

❖ ***Optimization of factors for inhibition efficiency (IE%)***

Screening experiments displayed that temperature and ICE concentration had a remarkable effect on the corrosion inhibition efficiency. So they were chosen as parameters in this investigation. Weight loss studies revealed that corrosion inhibition efficiency was upgraded in HCl medium than in H_2SO_4 medium. That motivated us to consider HCl solution as an acid medium. The design structure showing experimental results and predicted response for the test factors of central composite design (CCD) are summarised in Table 3.8.

A total of 9 experimental runs were performed in it. It was exhibited that corrosion inhibition efficiency improved tremendously with the increase in ICE concentration. The better inhibition efficiency that has been attained in this method was with 5 v/v% ICE concentration at 313 K working temperature. The proper combination of the two factors can be evaluated using RSM to get good inhibition efficiency. The

regression model satisfied the test factors and the inhibition efficiency shown in the quadratic equation (52).

$$IE = 10740 - 64.7X_1 + 32.8X_2 + 0.0976X_1^2 - 0.632X_2^2 - 0.075X_1X_2 \quad (52)$$

Using this quadratic equation, Analysis of variance (ANOVA) was then performed. ANOVA results having a significance level of 95% are displayed in Table 3.9.

Table 3.8: Experimental and predicted IE% from the weight loss measurements and CCD

Temp (X_1)	Conc (X_2)	IE%		Residual
		Experimental	Predicted	
313	5	88.93	81.4994	7.4306
333	1	37.39	24.8594	12.5306
313	1	69.18	59.3674	9.8126
333	5	51.14	40.9914	10.1486
313	3	86.27	72.9614	13.3086
323	5	66.03	51.4854	14.5446
333	3	46.2	35.4534	10.7466
323	1	41.85	32.3534	9.4966
323	3	52.38	44.4474	7.9326

Table 3.9: Analysis of variance for corrosion inhibition efficiency

Source	DF	Adj SS	Adj MS	F-Value	P-Value
Model	5	2770.86	554.17	37.43	0.007
Linear	2	2558.35	1279.18	86.39	0.002
Temp	1	2003.85	2003.85	135.33	0.001
ICE Conc	1	554.50	554.50	37.45	0.009
Square	2	203.51	101.76	6.87	0.076
Temp*Temp	1	190.71	190.71	12.88	0.037
ICE Conc*ICE Conc	1	12.80	12.80	0.86	0.421
2-Way Interaction	1	9.00	9.00	0.61	0.492
Temp*ICE Conc	1	9.00	9.00	0.61	0.492
Error	3	44.42	14.81		
Total	8	2815.29			

DF: degrees of freedom, Adj SS: adjusted sum of squares, Adj MS: adjusted mean of squares, F: Fischer's F-test value, P: probability

The noticeable parameter is the P-value in this Table which points out the significance of a factor on response. The degree of essentialness (α) was 0.05. It revealed

that the value of P was smaller than 0.05 for the two linear and one of the square terms. Among linear terms, the temperature was more significant than the ICE concentration. Square term of temperature is the only considerable term involved in squared terms. Pareto chart[155] (Fig. 3.18) also illustrates the significance of linear and non-linear terms on inhibition efficiency. The linear terms, such as temperature and ICE concentration, have a remarkable effect on the inhibition efficiency. In contrast, the square term of temperature has less influence on the response. Square term of ICE concentration and the two-way interaction term X_1X_2 have little effect on inhibition efficiency, same as ANOVA.

Accuracy of this quadratic model can be proved by Residual plots, as shown in Fig. 3.19. Normal probability plot conveyed that the residual distribution is normal since the residuals were merged into the straight line. Histogram of residuals represented that the residuals are distributed in a symmetric manner at all frequencies[156]. Versus order plot exhibited that observed runs were scattered within the fixed area of residuals which confirmed the accuracy of the regression model.

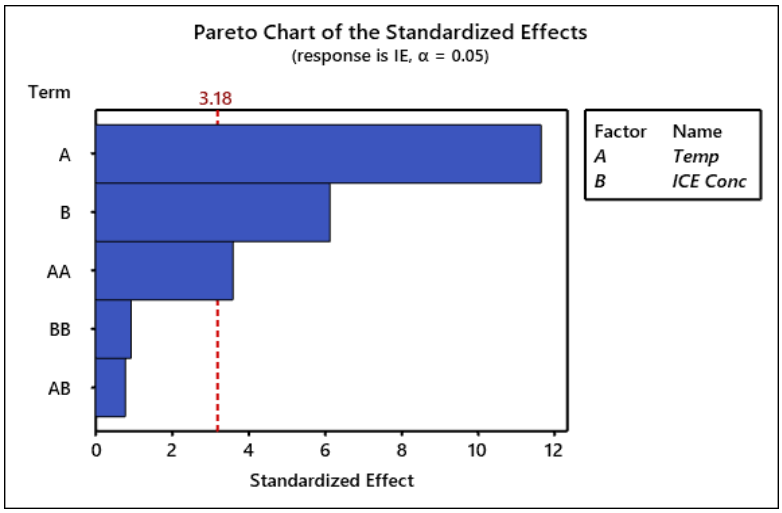

Fig. 3.18: Pareto chart of the standardized effects of mild steel

The perfect model for experimental results was inferred by agreeing to R^2 and R^2(adj) values to unity. In the present work, the R^2 and R^2(adj) values were 0.9842 and

0.9579, respectively, showing the most suitable predicted model for experimental values. Therefore, the results can be accurately analyzed by the model.

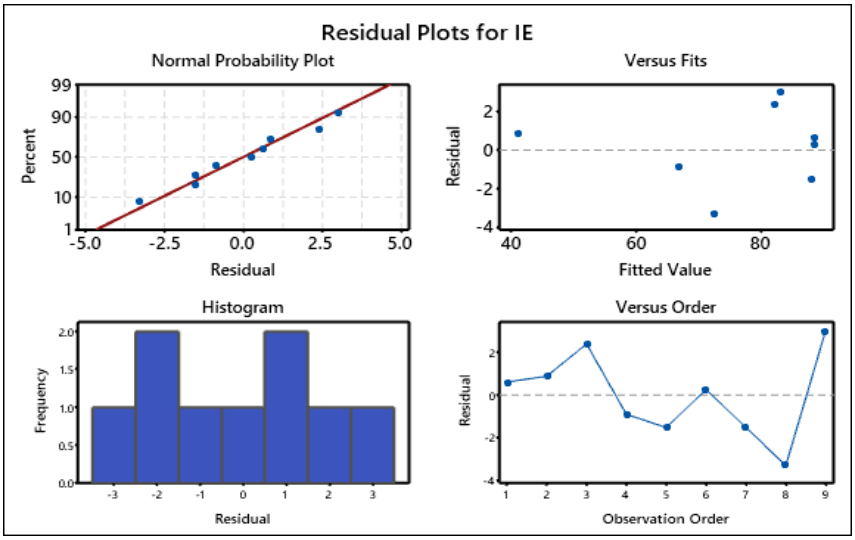

Fig. 3.19: Residual plots for inhibition efficiency

Main effects plots elucidate the effect of factors on the response. Fig. 3.20 shows the main effects plots for the fitted means of inhibition efficiency. Fig. 3.20 exhibited the highest inhibition efficiency reached at 5 v/v% concentration of ICE and at 313 K working temperature. At elevated temperatures, the kinetic energy of the inhibitor molecules increased, and the number of collisions between the molecules also enhanced. When the temperature goes up, the adsorbed film formed by the inhibitors on the metal surface is destroyed and thus, inhibition efficiency decreases. Whereas inhibition power of ICE and its concentration is directly proportional to each other. The corrosion rate was lowered in the presence of ICE molecules. As the concentration is added, the adsorption on the metal surface is enhanced and thus exhibits increased inhibition efficiency.

Contours and 3-D surface plots show the interconnection between the factors[157] and IE (%), represented in Fig. 3.21. It was worth mentioning that the inhibition efficiency goes up with ICE concentration for a particular temperature. But, inhibition efficiency and temperature are inversely proportional to each other. This relationship can

be attributed to the physical interaction between ICE molecules and the mild steel surface.

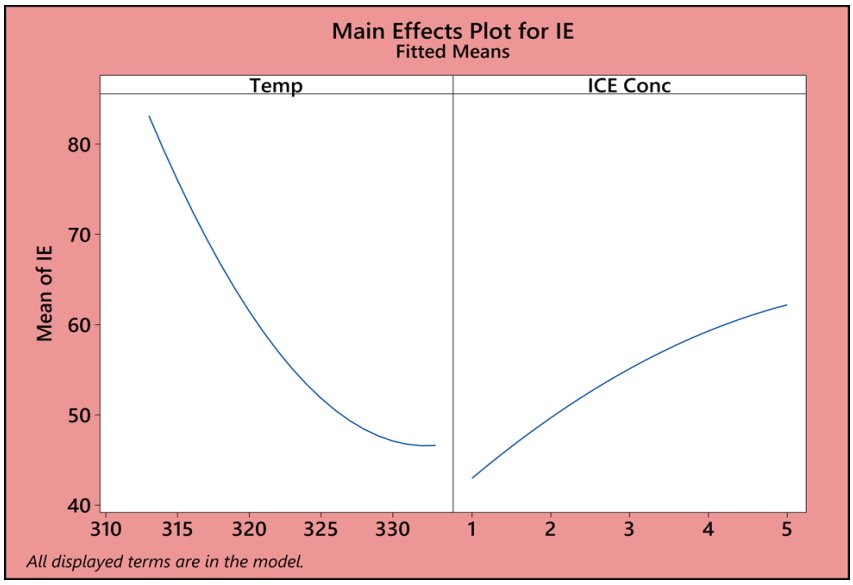

Fig. 3.20: Main effects plots for inhibition efficiency of mild steel in HCl medium

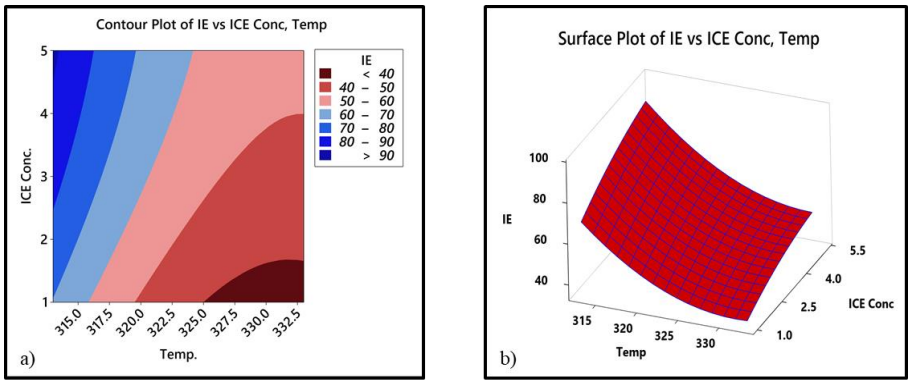

Fig. 3.21: a) Contour and b) 3-D surface plot for inhibition efficiency

❖ ***Response optimization***

Well organized quadratic equation (52) was used to optimize the independent factors such as temperature and ICE concentration to derive maximum IE (%). For the most feasible response, the desirability function method was applied. Response optimization plot for IE is exhibited in Fig. 3.22. The optimized conditions for best IE (%) identified were temperature (313 K) and ICE concentration (5 v/v %) for the HCl environment, and the corresponding predicted IE was 91.73 %, as given in Fig. 3.22.

Confirmation tests helped to verify the recurrence of the experimental outcomes and approve the accuracy of the model.

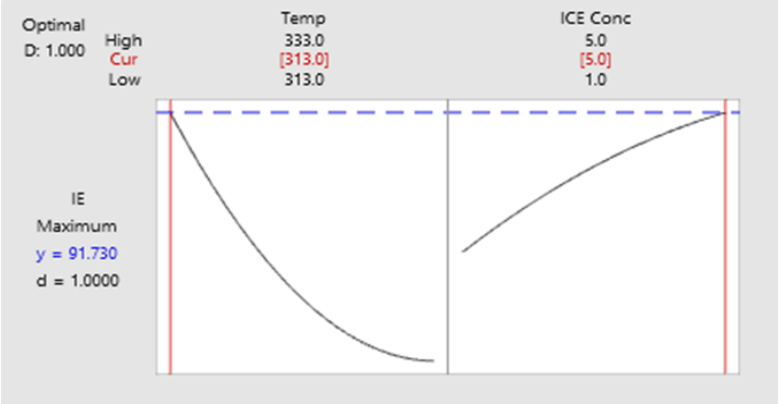

Fig. 3.22: Response optimization plot for inhibition efficiency

Conclusions

- *Ixora coccinea* leaf extract (ICE) acts as an efficient green inhibitor for corrosion of mild steel in 1 M HCl and 0.5 M H_2SO_4 medium. As the concentration of the inhibitor increases, the protecting power also increases. Temperature and inhibition efficiency are in inverse proportional relation
- On comparing, ICE in HCl medium shows higher efficiency than H_2SO_4 medium.
- Probability for the complexation of ICE with metal ions is confirmed by UV-Visible spectral studies.
- Electrochemical impedance analysis exhibits that charge transfer resistance increases and double layer capacitance decreases according to ICE concentration.
- Potentiodynamic polarization measurements exhibit mixed type character of ICE towards corrosion inhibition.
- Quantum mechanical calculations of ixorene, a major component present in ICE, supports the inhibition power of ICE.
- The adsorption studies of ICE shows that it obeys Langmuir adsorption isotherm.
- Surface morphological studies also confirmed the protecting power of ICE.

- Statistical analysis also verified the effect of temperature and concentration on inhibition efficiency of ICE towards mild steel corrosion.